PLANETARY SCIENCE

Rapid topographic growth of the Taiwan orogen since ~1.3–1.5 Ma

Queenie Chang[1,2]*, Michael T. Hren[1], Larry Syu-Heng Lai[3,4], Rebecca J. Dorsey[3], Timothy B. Byrne[1]

We present the first paleotopographic reconstruction of Taiwan by measuring the hydrogen isotope composition of leaf waxes (δ^2H_{nC29}) preserved in 3-Ma and younger sediments of the southern Coastal Range. Plant leaf waxes record the δ^2H of precipitation during formation, which is related to elevation. Leaf waxes produced across the orogen are transported and deposited in adjacent sedimentary basins, providing deep-time records of the source elevation of detrital organic matter. δ^2H_{nC29} exported from the southern Taiwan orogen decreased by more than 40‰ since ~1.3–1.5 Ma, indicating an increase of >2 kilometers in the organic source elevation. The increase in organic source elevation is best explained by rapid surface uplift of the southern Central Range at around ~1.3–1.5 Ma and indicates that this part of the orogen was characterized by maximum elevations of at least 3 km at this time. Further increase in organic source elevation from ~0.85 to ~0.3 Ma indicates continued topographic growth to modern elevations.

INTRODUCTION

The topography of mountain belts reflects the balance between rock uplift and erosion (*1*). This balance is influenced by the interactions among tectonics, climate, surface erosion, and global carbon cycling (*2*, *3*). Tropical mountain belts are often characterized by high rates of precipitation, erosion and organic carbon export, as well as high rates of rock weathering (*4*–*8*). Recent studies have suggested that exhumation and erosion of Southeast Asian tropical mountain belts may be a key mechanism for Neogene cooling due to feedbacks among uplift, global silicate weathering rates, and atmospheric CO_2 (*8*). However, others suggest that tropical mountains may serve as a carbon source rather than sink (*7*, *8*), and this subject remains debated (*9*). One of the key limitations to quantifying the role of tropical mountain building in the global carbon cycle is that there are few records of paleotopography for these systems. Here, we present a record of the source elevation of organic matter exported from Taiwan, an active orogenic mountain belt characterized by some of the highest rates of erosion, chemical weathering, and sediment export on the globe (*4*).

The Taiwan mountain system was formed over the past ~5 Ma due to collision between the Philippine Sea plate and Eurasian plate (*10*). A longstanding interpretation of mountain building in Taiwan postulates initial surface uplift in the north with southward propagation of topography during Plio-Pleistocene time, with the northern two-thirds of the Central Range of Taiwan reaching a steady-state balance among exhumation, uplift, and erosion by the present (*11*, *12*). Thermochronology data show that the Taiwan orogenic belt has undergone multiple accelerations in the rate of rock exhumation through its orogenic history (*13*–*18*). Before 2 Ma, the Taiwan mountain belt is argued to have been characterized by low exhumation rates and an early phase of removal of the sedimentary cover (*13*, *17*, *18*). Zircon (U-Th)/He and fission-track ages of the Central Range metamorphic core indicate complicated patterns of rock deformation and low exhumation rates before 2 Ma (<1.0 mm/year) (*13*, *18*). Low exhumation rates are consistent with detrital zircon records in foredeep basin sedimentary rocks of the Coastal Range, which show that zircon fission-track data in 2- to 4-Ma-old syn-orogenic foredeep basin sediments were not reset and the onset of acceleration is at ~3.5 to 2.5 Ma (*17*).

Zircon fission-track and (U-Th)/He ages in metamorphic core and foredeep basin rocks show notable increases in exhumation rate (2.3 to 6.5 mm/year) at ~2 Ma (*13*, *17*, *18*), and sediment accumulation records from the foredeep basins in the Coastal Range show a similar increase in sedimentation rate at this time (*19*, *20*). Apatite (U-Th)/He ages indicate a further increase in exhumation to ~4 to 8 km/Ma from 0.5 Ma to the present (*13*, *15*, *16*). The youngest phase of rock exhumation (<0.5 Ma) is coincident with the rapid uplift and basin inversion in the Coastal Range (*20*) and the eastward migration of the depositional center in eastern Taiwan over the past half million years (*21*).

Although thermochronology and sediment data both record post-Pliocene acceleration of exhumation and erosion, there presently are no direct constraints on the paleotopography of Taiwan. As a result, there is considerable debate over the time scale and duration of landscape adjustment in response to accelerated rock exhumation and mass redistribution by surface processes (*22*). Here, we measure the hydrogen isotopic composition of sedimentary/detrital leaf waxes ($\delta^2H_{leaf\text{-}wax}$) preserved in Plio-Pleistocene syn-orogenic sediments of the southern Coastal Range of Taiwan (Fig. 1) to constrain changes in organic source elevation through time. These data are related to catchment hypsometry (*23*) and provide the first constraints on the evolution of paleotopography in the Taiwan mountain range.

$\delta^2H_{leaf\text{-}wax}$ has been used to reconstruct the paleoelevation history of mountains, because it records the isotopic composition of ancient precipitation (*23*–*25*), which, in turn, is related to surface topography. Because atmospheric moisture encounters an orographic barrier, it can undergo orographic lifting that results in cooling and condensation. Progressive removal of water vapor during lifting produces a systematic decrease in δ^2H of precipitation

[1]Department of Earth Sciences, University of Connecticut, Storrs, CT, USA. [2]Earth and Environmental Sciences Department, Denison University, Granville, OH, USA. [3]Department of Earth Sciences, University of Oregon, Eugene, OR, USA. [4]Department of Earth and Space Sciences, University of Washington, Seattle, WA, USA.
*Corresponding author. Email: queenie.chang@uconn.edu

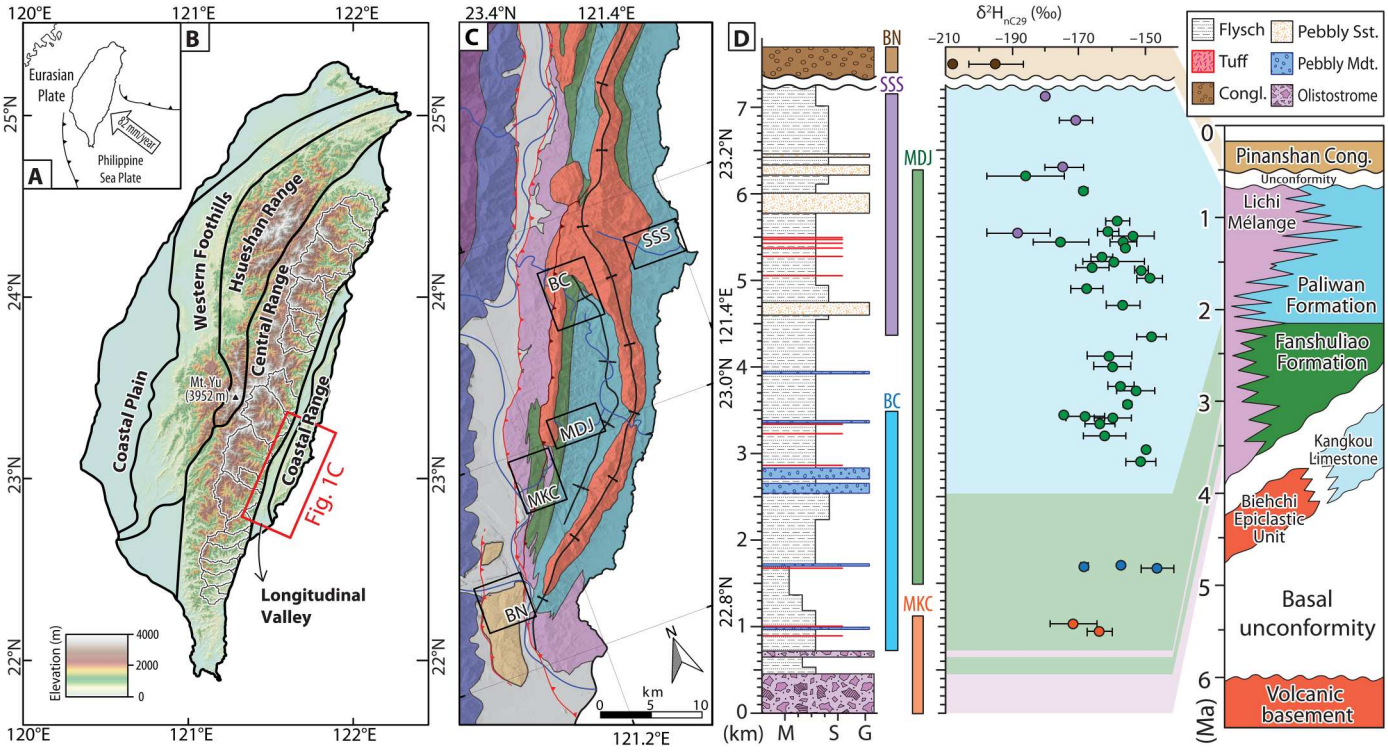

Fig. 1. Geographic map of Taiwan and geological map and stratigraphic framework of the southern Coastal Range. (**A**) Simplified tectonic framework in Taiwan. (**B**) Geographic map of Taiwan. Major catchments in eastern Taiwan are outlined with thick black lines. (**C**) Geological map of the southern Coastal Range of Taiwan. Black boxes show the sampled sections: Beinan tableland (BN), Mukeng River (MKC), Bieh River (BC), Madagida River (MDJ), and Sanshian River (SSS). See figs. S2 and S3 for detailed geological maps and sample locations. (**D**) Stratigraphic framework and composite column of the southern Coastal Range with projected positions of δ^2H_{nC29} (hydrogen isotope composition of leaf waxes) data. ‰, per mil. See fig. S1 for detailed stratigraphic columns and sample locations.

(*26*). Plants can incorporate ambient water into organic molecular biomarkers such as fatty acids or *n*-alkanes, which are abundantly produced in epicuticular waxes and record the isotope composition of precipitation (*24*). The isotopic composition of leaf wax molecular biomarkers that are accumulated in soils or sediments can therefore record isotope hydrology, which reflects both climate and topography.

Plant biomarkers are produced by a range of organisms across a landscape and are abundantly preserved in soils and sediments. We collected 39 siltstones and mudstones samples from orogen-derived deposits in ~3- to 0.78-Ma marine turbidites of the Fanshuliao and Paliwan formations and ~0.3-Ma fluvial deposits of the Pinanshan Conglomerate of Fig. 1 in the southern Coastal Range of eastern Taiwan to analyze the hydrogen isotope composition of terrestrial organic matter exported from the orogen. These data are then coupled with a precipitation isotope model to reconstruct the source elevation of organic matter exported from Taiwan drainages and used to infer topographic evolution of this orogen. Biomarker samples were collected from five sections that span ~30 km along the strike of the eastern Taiwan orogenic belt. These sections are Beinan tableland (BN), Sanshian River (SSS), Madagida River (MDJ), Bieh River (BC), and Mukeng River (MKC) sections (Fig. 1 and figs. S1 to S3). The lithostratigraphic descriptions and age constrains follow Lai *et al.* (*19*).

In this study, we focus on the isotopic record of *n*-alkanes with 29 carbon atoms (nC_{29}), as this compound is the most abundant molecular species in the soil and sediments in Taiwan (*23*). Modern Taiwan soils show a δ^2H_{nC29} (hydrogen isotope composition of leaf waxes) of approximately −150 to −155 per mil (‰) near sea level and less than −200‰ at elevations of >2500 m, yielding an ~20‰ per km decrease in δ^2H_{nC29} that mirrors the $\Delta\delta^2H$ of precipitation across the entire elevation range of the Taiwan orogen (*23*). These molecules can be accumulated in soil and be eroded, ablated by wind/rain, or mobilized by rain that moves organics through surface and groundwater as well as transported through river networks and deposited in fluvial and marine environments (*24*). These leaf waxes molecules are capable of carrying and preserving isotopic signatures from their high-elevation sources (*23*, *27*–*29*). In Taiwan, the average residence time of organic carbon and, in particular, plant biomarkers is generally short (<1000 years) so the carbon that is exported is representative of the integrated carbon produced across the landscape (*30*). Studies have shown that modern river sediments δ^2H_{nC29} data in Taiwan generally reflects the hypsometry of leaf waxes produced throughout a catchment (i.e., catchment mean elevation) (*23*).

RESULTS

The δ^2H_{nC29} of detrital leaf wax biomarkers preserved in 3 Ma and younger sedimentary rocks show at least three distinct groupings of decreasing value from the Pliocene through Mid-Pleistocene (Fig. 2A) with a total mean decrease of more than 40‰. Before ~1.5 Ma, the mean δ^2H_{nC29} of detrital leaf waxes in the Pliocene-aged Fanshuliao and Paliwan formations is approximately −160‰ and

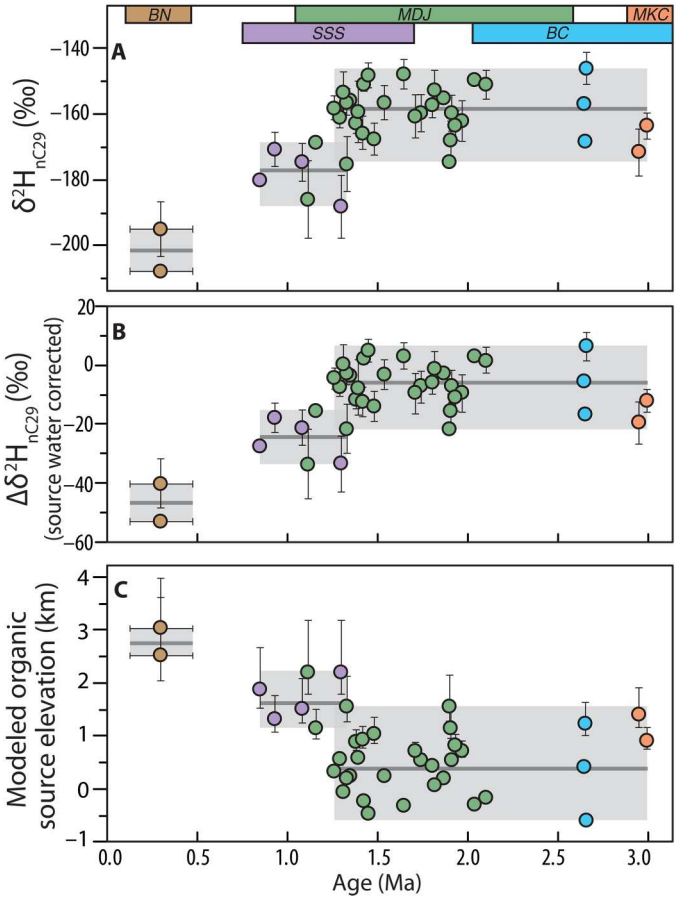

Fig. 2. Detrital leaf wax δ^2H_{nC29} data and interpreted source elevations. (**A**) δ^2H_{nC29} values. (**B**) Source water–corrected $\Delta\delta^2H_{nC29}$ values. (**C**) Interpreted organic source elevations of $\Delta\delta^2H_{nC29}$ values based on a one-dimensional (1D) thermodynamic atmospheric model (*31*, *32*). Colored circles represent samples from matching stratigraphic sections at the top of (A); bar length represents temporal coverage of individual sections. Gray shading and thick gray lines show the mean value and ranges of the three distinct grouping of numbers.

ranges from −148 to −174‰ (similar to modern low-elevation soil δ^2H_{nC29}). Between ~1.3 and 1.5 Ma, most individual δ^2H_{nC29} values remain high (similar to before 1.5 Ma), but depleted isotopic signatures as low as −175 (18TW- MG19) and −188‰ (18TW-SS01) are first observed. From ~1.3 to ~0.85 Ma, the mean δ^2H_{nC29} in the upper Paliwan Formation decreases to approximately −180‰, with values as negative as −186‰. From ~0.85 to ~0.3 Ma, extremely depleted values (−195 and −208‰) are observed in Mid-Late Pleistocene deposits of the Pinanshan Conglomerate, with a mean of −201‰.

While a number of factors could influence sedimentary δ^2H_{nC29}, including degradation, reworking of older materials, and changes in climate/ecosystem, we argue that these factors are a second-order effect on detrital leaf wax δ^2H_{nC29} and instead our data reflect primary isotopic signatures, which, in turn, reflect organic source elevation. There are two reasons for this: (i) The stratigraphic sections of the southern Coastal Range analyzed here have undergone minimal burial heating, and the exposed metamorphic rocks of the eastern Central Range have minimal to no nC_{29}-alkanes that could bias our record; and (ii) the subtropical climate of Taiwan has remained relatively constant since the Pliocene (see Materials and Methods). As a result, we argue that leaf wax isotopes reflect the primary isotopic signatures of fluvially transported leaf waxes from the evolving orogen.

On the basis of modern δ^2H_{nC29} and isotope-elevation relationships, the observed >40‰ decrease in leaf wax δ^2H_{nC29} for the past 3 Ma is best explained by an increase in organic source elevation at ~1.3–1.5 Ma. To quantify the changes in source elevation detected in the isotopic data, we apply a one-dimensional (1D) thermodynamic precipitation isotope model (*31*, *32*) to estimate the changes in precipitation isotopic composition ($\Delta\delta^2H$) as a function of elevation. We use the post-industrial Taiwan mean annual temperature (296 K) and relative humidity (80%) as sea level starting conditions. Model predictions closely match the observed $\Delta\delta^2H_{nC29}$ and $\Delta\delta^2H$ in modern soil and river waters in Taiwan (Fig. 3) (*23*).

Relating δ^2H_{nC29} to paleoelevation requires an understanding of both the magnitude of change in δ^2H ($\Delta\delta^2H$) as a function of elevation and an estimate of sea level precipitation isotopes (base level) through time. Base-level precipitation hydrogen isotopes in Taiwan are to first order, controlled by climate and ocean δ^2H composition. Climate (i.e., temperature) influences base-level precipitation isotopes due to impacts on source water composition, the temperature dependence of isotope fractionation, evaporation, and rainfall intensity (*26*). The sea surface temperature of the South China Sea decreased by ~3°C from 3 Ma to the present (*33*); however, temperatures were possibly cooler during peak glacial intervals. Global climate model simulations and biomarker δ^2H data both show that regional warming of 4° to 6°C from the last glacial maximum to interglacial produces a change in precipitation/leaf wax δ^2H of <10‰ (*34*). Thus, Pliocene to recent climate variability is unlikely to produce a substantial change in base-level precipitation δ^2H during the time scale of our data.

Plio-Pleistocene growth of Northern Hemisphere ice sheets has increased seawater δ^2H through time and likely affected the isotopic composition of surface water in the moisture source regions for

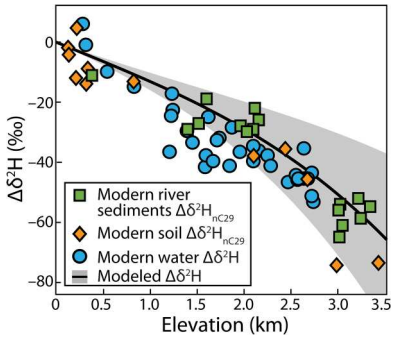

Fig. 3. Model-predicted $\Delta\delta^2H$ as a function of elevation. Model predictions closely match modern observed soil and river sediments $\Delta\delta^2H_{nC29}$ and water $\Delta\delta^2H$ data in Taiwan reported by Hren and Ouimet (*23*). Note that modern soil $\Delta\delta^2H_{nC29}$ are plotted against sample site elevation, while the modern fluvial sediments $\Delta\delta^2H_{nC29}$ and river water $\Delta\delta^2H$ are plotted against catchment mean elevation. The thick black line and gray shading show the modeled $\Delta\delta^2H$-elevation relationship and 95% confidence interval based on the 1D thermodynamic model (*31*, *32*) with starting condition similar to low-elevation areas (296 K, relative humidity: 80%).

Taiwan. We correct for the effect of changing ice volume on source water δ^2H using planktonic foraminifera $\delta^{18}O$ and $U^{k'}_{37}$ sea surface temperature records from Ocean Drilling Program (ODP) site 1148 in the South China Sea. We apply this correction to leaf wax data to account for potential changes to base-level precipitation (see Materials and Methods) (*33*, *35*). We use the source water–corrected $\Delta\delta^2H_{nC29}$ (Fig. 2B) and modeled $\Delta\delta^2H$-elevation relationships (Fig. 3) to reconstruct the predicted source elevation of terrestrial organic matter exported from the Taiwan orogenic belt for the past 3 Ma (Fig. 2C).

DISCUSSION

Organic source elevation

There are three distinct δ^2H_{nC29} groupings observed within our record. Before ~1.3–1.5 Ma, the mean detrital biomarker δ^2H_{nC29} is approximately −160‰. On the basis of modern river sediments δ^2H_{nC29} and modeled precipitation $\Delta\delta^2H$-elevation relationships (Fig. 3), these values are consistent with compositions of organic matter sourced from low elevations ~0.5 km (Fig. 2C). However, several samples before ~1.3–1.5 Ma have δ^2H_{nC29} values consistent with organic source elevations as high as 1 km. In the second grouping, which records the interval from ~1.3 to ~0.85 Ma, the mean detrital δ^2H_{nC29} decreases to approximately −180‰, suggesting an increase in organic source elevation to ~1.5 km (Fig. 2C). The final group is captured by sediments within the Pinanshan Conglomerate at ~0.3 Ma. δ^2H_{nC29} data from these conglomerate deposits are consistent with an increase in organic source elevation to >2.7 km (Fig. 2C).

The molecular biomarkers preserved in sediments can be contributed from a range of elevations within a catchment, and these contributions may not be homogeneous (*23*). The observed decrease in organic matter δ^2H_{nC29} in ~1.3–1.5 Ma and younger sediments unambiguously reflects an increased proportion of organic matter derived from higher elevations after this time. The key question is how this increase in organic source elevation relates to changes in topography and the elevation of the southern Central Range of Taiwan? Below, we discuss the factors that influence organic source elevation and how this relates to topography.

The first marked decrease in δ^2H_{nC29} values is observed at ~1.3–1.5 Ma within Paliwan Formation sediments. This isotopic shift is not associated with distinct changes in sedimentary process, depositional system, or paleobathymetry (*19*, *20*). Thus, it is unlikely that the shift in δ^2H_{nC29} is caused by a change in depositional phase or proximity to the orogen.

Modern Taiwan δ^2H_{nC29} data show that variations in catchment hypsometry and detrital organic source elevation are the primary control on δ^2H_{nC29} of fluvially transported organic matter in this setting (*23*). Thus, the simplest interpretation of decreasing δ^2H_{nC29} through time is a shift in organic source elevation. There are several possible mechanisms that could affect the observed decrease in δ^2H_{nC29} that first appears within the Paliwan Formation. These include: (i) increased production/export of organic material in high-elevation areas within the source catchment due to changing climate or erosion, (ii) reorganization of catchments/drainage capture that results in a change in organic matter source regions, and (iii) an increase in the surface elevation of the source catchment for contributing terrestrial organic matter.

Detrital δ^2H_{nC29} does not provide a direct measure of the height of an orogen but rather the elevation distribution of organic matter exported from source to sink. Thus, factors that influence the movement of organic matter from source to sink can bias the isotopic signal preserved in depositional sites. Surface uplift affects hillslope and mass wasting processes that tend to occur at greater frequency in steep-sloped terrain and higher elevation regions of a catchment (*36*). In Taiwan, frequent earthquakes may also play a role in reducing hillslope stability. Both of these factors have the potential to increase the proportion of high-elevation sediments exported from an orogen (*37*). However, sediment generation and export is not the same as organic carbon export. The spatial pattern of carbon export from a catchment is likely different from the spatial pattern of sediment export due to factors such as carbon production (plant productivity) and storage. Plio-Pleistocene warming could also change the rate of production of *n*-alkanes as a function of elevation, which could alter the proportion of high- or low-elevation nC_{29} in fluvial sediments. Both of these factors could affect the elevation-dependent relationship between molecular production and export and could bias detrital δ^2H_{nC29} toward more negative values. However, models of variable elevation-dependent erosion and primary production functions in Taiwan show that the bias on δ^2H_{nC29} of integrated organics is less than ~10‰ (*23*).

Changes in the contributing catchments or catchment geometries have the potential to alter the source of organic matter exported via river networks. These changes could alter detrital leaf waxes δ^2H_{nC29} values and resultant interpretations of organic source elevations represented by these values. The stratigraphic sections sampled as part of this work range from marine turbidites to fluvial conglomerates and are all located within <30 km of each other. If measured sedimentary deposits were heavily biased by inputs from individual catchments, then temporal changes in drainage networks could bias the observed organic δ^2H signal, if these catchments have distinct δ^2H_{nC29}. Nevertheless, modern Taiwan topography shows that catchments located adjacent to one another tend to be characterized by similar catchment mean and maximum elevations (Fig. 4). Thus, although changes in drainage networks during uplift could introduce some degree of variability in the δ^2H_{nC29} of exported organics, these are likely small effects. Furthermore, Fanshuliao and Paliwan formations sediments are turbidite deposits that probably represent part of a submarine fan complex with a source are larger than a single watershed. These sedimentary rocks, therefore, contain a mix of sediment and organic matter exported from across the eastern flank of the Taiwan mountain belt and capture regional exhumation history rather than sediments from a single catchment. We interpret terrestrial leaf wax δ^2H_{nC29} preserved in marine units to reflect regional source elevation.

Last, headwater incision into existing topography or stream capture events could produce episodic increases in sediment and organic source elevation for exported organics (*38*). For example, in the modern southeastern Central Range, the Luliao catchment (catchment no. 8 in Fig. 4) is interpreted to be eroding into two other larger catchments, Luye (catchment no. 7 in Fig. 4) and Hsinwulyu (catchment no. 9 in Fig. 4). One might consider that this ongoing capture event would produce a large isotopic signature in exported leaf wax δ^2H_{nC29}. However, from a geomorphic standpoint, merging of these three catchments would only increase catchment mean elevation from around 1.4 to 1.7 km, which is an ~300-

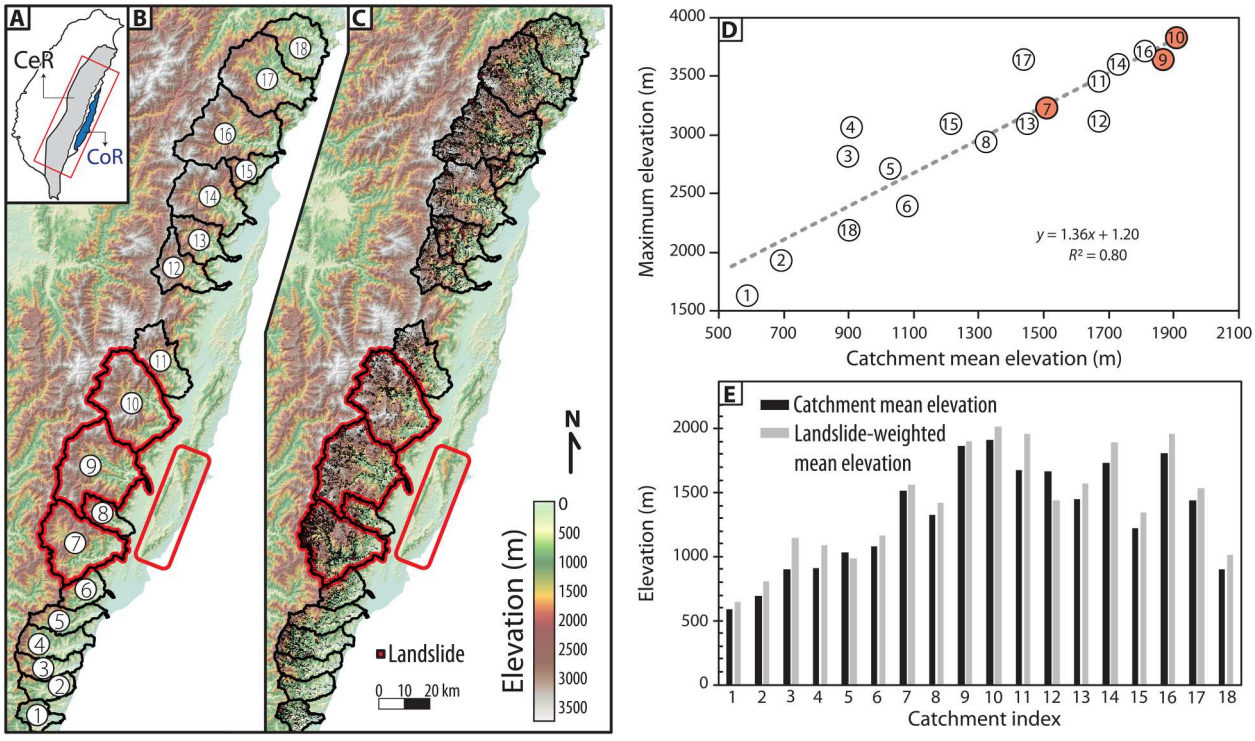

Fig. 4. Modern catchment hypsometry in eastern Central Range and the comparison among catchment mean elevation, maximum elevation, and landslide-weighted mean elevation. (**A**) The location of analyzed catchments and study area. CeR, Central Range; CoR, Coastal Range. (**B**) A total of 18 catchments are analyzed. Red rectangular box indicates the study area. Catchments outlined in red (catchment nos. 7, 9, and 10) are considered the dominant catchments that contribute sediments and organic matter to the study area in modern day. (**C**) The modern-day distribution of landslides within the analyzed catchments. The landslides data are from Lin *et al*. (*64*). (**D**) The relationship between catchment mean elevation and maximum elevation. R^2, coefficient of determination. (**E**) Comparison between catchment mean elevation and landslide-weighted mean elevation show that hillslope processes could shift the source of sediments and organic matter to higher-elevation region by at most a few hundred meters.

m increase in sediments/organic source elevation, an expected shift in δ^2H_{nC29} of only 6 to 7‰. Thus, we argue that past drainage capture events may contribute to some of the observed short-term variations in detrital leaf wax δ^2H_{nC29} but are not sufficient to explain the ~20‰ shift in δ^2H_{nC29} at ~1.3–1.5 Ma and further decreases in δ^2H_{nC29} observed between ~0.85 and ~0.3 Ma.

The large decreases in detrital δ^2H_{nC29} at ~1.3–1.5 Ma is consistent with an increase in organic source elevation from ~0.5 to ~1.5 km and is best explained by topographic growth of the Taiwan orogen around this time. Modern river sediments show that δ^2H_{nC29} of detrital organics reflects the mean elevation of contributing organic matter sources (i.e., for Taiwan, the catchment mean elevation) (Fig. 3). An analysis of modern eastern Taiwan river catchments shows that drainages with catchment mean elevations of ~0.5 km are generally characterized by high relief with maximum peak elevations of up to ~1.9 km. Catchments with mean elevation of ~1.5 km generally show peak elevations of >3 km (Fig. 4). Our δ^2H_{nC29} data show that before ~1.3–1.5 Ma, the mean catchment elevation recorded by detrital organics was ~0.5 km. If catchments were characterized by similar hypsometries to modern, then this indicates that maximum elevations (mountain height) were on the order of 2 km at this time. We note that that there are several δ^2H_{nC29} values within the section that indicate organic source elevations as high as 1.5 km before ~1.3–1.5 Ma. Infrequent short-term variations in δ^2H_{nC29} such as described above, are most likely caused by variations in short time scale surface processes such as climate or tectonic-driven erosion events or catchment reorganization. After ~1.3–1.5 Ma, δ^2H_{nC29} values show a consistent decrease by ~20‰, indicating an increase in the organic source elevation to 1.5 km. If the detrital organic signature reflects a catchment mean elevation similar to modern Taiwan rivers, then this indicates a phase of rapid growth of the Taiwan orogen and an increase in maximum elevations to >3 km by 1.3 Ma.

The second major detrital leaf wax δ^2H_{nC29} decrease occurs in our data between ~0.85 and ~0.3 Ma, with a decrease from approximately −180‰ to a mean of −201‰ in Pinanshan Conglomerate (Fig. 2A). These exceptionally low δ^2H_{nC29} values can only be produced by contributions from organic matter produced at high elevations and are consistent with a source elevation of up to ~2.7 km (Fig. 2C). If the source elevation recorded by organic matter geochemistry reflects the catchment mean elevation at ~0.3 Ma, similar to the relationship between leaf wax δ^2H_{nC29} and catchment hypsometry observed in modern Taiwan rivers (Fig. 4), then it would indicate a much higher catchment mean elevation at that time than modern Taiwan. From a geodynamic or an erosional standpoint, this is questionable and suggests other factors are required to explain to these very negative values.

First, the proximity of depositional sites to the orogen influences the catchment hypsometry and could affect detrital δ^2H_{nC29} values. The Pinanshan Conglomerate is composed of rounded fluvial

gravels of metamorphic rocks from the Central Range, indicating a depositional environment close to the orogen. Such proximal depositional sites to the mountain range could have collected a larger proportion of sediments and organic matter from higher elevation regions, resulting in lower detrital leaf wax δ^2H_{nC29} values. In contrast, distal sites may collect more organics from low-elevation coastal plain regions. In this manner, depositional setting could impose a bias in the apparent relationship between detrital organic δ^2H_{nC29} and catchment hypsometry. The effect would be an overestimate of catchment mean or maximum elevation. However, we argue that this is a minimal factor for eastern Taiwan because of limited coastal plain area and steep catchments in eastern Taiwan during the entire period of sediment deposition. According to lithofacies analysis and paleogeographic reconstruction (*19*, *20*), the Coastal Range sedimentary strata that we studied were deposited in a retro-foredeep basin. Abundant submarine mass-wasting deposits (i.e., the Lichi Mélange) are interpreted to have been deposited at the base of slope to proximal basin plain. This suggests that the foredeep basin in the southern Coastal Range was directly adjacent to and east of a steep orogenic front, with limited coastal plain and continental shelf and sediments were derived. Paleocurrent and paleoslope data indicate that nearly all sediments deposited in our sample sites were derived from the eastern retrowedge of the main orogen to the west/northwest of the basin (*19*).

Second, changes in patterns of erosion or elevation-related erosion could bias detrital δ^2H_{nC29} signals. If the detrital organic matter was sourced homogeneously from the river catchments, then the exceptional negative δ^2H_{nC29} values recorded in the Pinanshan Conglomerate indicate that by ~0.3 Ma, the organic source elevation (which in the modern approximates catchment mean elevation) in eastern Taiwan may have been as high as 2.7 km. On the basis of modern catchment hypsometries, maximum topographic elevations for such catchments would be much higher than the modern orogen. Were the mountains of the southern Central Range higher at 0.3 Ma than present? Is this signature biased by an increase in erosion/export from high elevations in the catchment? We cannot exclude the possibility that the shift to highly depleted organic δ^2H_{nC29} values reflect an increase in the proportion of high-elevation organic matter due to nonuniform erosion processes affected observed δ^2H_{nC29} values. Hillslope processes such as landslides that produce sediment from high-elevation regions are likely to become more frequent as the height of an orogen increases (*36*, *39*, *40*). The high energy system represented by the conglomerates may capture a shift to greater mass wasting/erosion from these high-elevation regions of the orogen. However, there are two reasons that we do not believe that this controls the observed shift to highly depleted δ^2H_{nC29} values. First, the export of organic carbon is not directly coupled to sediment production in Taiwan. This region is characterized by thin soils, minimal storage, and short residence times (*30*). In addition, organic molecules are mobilized by both physical erosion and chemical mobilization and moves with soil and groundwater. Thus, it is possible to move organic molecules downslope even if there is not movement of sediment. Second, we examine the effect of a change in elevation-dependent erosion on detrital δ^2H_{nC29} and note that the difference in calculated sediment source elevation for a scenario where sediment is produced evenly throughout a catchment independent of elevation and one in which sediment generation/erosion is weighted by the actual frequency of landslides within a catchment produces a difference of only a few hundred meters in the calculated mean elevation of sediment produced in the catchment (Fig. 4). Thus, even if organic biomolecular export were linked to physical erosion, it is unlikely that a change in landslide frequency could account for the observed >20‰ decrease in δ^2H_{nC29} values between ~0.85 and 0.3 Ma without a change in the overall elevation of the landscape.

Another possible explanation for inferred higher than modern catchment mean elevations in the Pinanshan Conglomerate is that the hypsometry of ancient Taiwan drainages was different from the modern. Multiple studies across Taiwan suggest that recent surface uplift resulted in the generation of high-elevation and low-relief landscapes, and some suggest that these surfaces of low relief may correspond to multiple stages of acceleration in observed exhumation (*13*, *18*, *41*–*43*). Uplift and erosion of these high-elevation and low-relief surfaces could result in a temporal change in the relationship between maximum elevations and the catchment mean elevation (hypsometry). The depleted signal that we capture in the conglomerate may simply reflect erosion into the uplifted low-relief and high-elevation Pleistocene surfaces. In total, the observed decrease in δ^2H_{nC29} value in the sedimentary record is best explained by a combination of continued growth of the Taiwan orogen through the Pleistocene and shift in organic source elevation toward higher elevation due to a change in catchment hypsometry, as rivers eroded into and dissected the recently uplifted terrain.

Mechanism of topographic growth in Taiwan

The δ^2H_{nC29} data show that the source elevation of detrital organic matter first shifts to consistently higher elevations at ~1.3–1.5 Ma. This increase in organic source elevation (i.e., equivalent to catchment mean elevation in the modern), records a phase of surface uplift of the Taiwan orogenic belt that begins sometime between 1.3 and 1.5 Ma. Biomarker data indicate that the increase in organic source elevation, which likely reflects surface uplift, occurs ~0.5 Ma later than observed increases in exhumation and sediments accumulation rates, which both increase at ~2 Ma (Fig. 5). Surface uplift reflects the balance between rock uplift and erosion. Increased surface uplift generally precedes an increase in erosion/exhumation. Our data show that topography grew rapidly after observed increases in exhumation and sediment accumulation rates (Fig. 5). This observation may indicate heterogeneity in the temporal pattern of uplift and exhumation across the Taiwan mountain belt and require future work at different portion of the orogen to explore.

Recent examination of rock fabrics from the metamorphic core of the Central Range indicates left lateral, strike-slip deformation at ~5 to 2 Ma (*44*). After 2 Ma, data indicate a transition to a period of vertical shortening and northeast-southwest (NE-SW) extension (*45*, *46*). Slip on a crustal-scale out-of-sequence thrust could be the primary mechanism for the exhumation of the Central Range (*18*). Plate reconstructions also suggest a change in plate convergence orientation from highly oblique to nearly orthogonal between 1 and 2 Ma (*47*), which could result in a transition from strike-slip to vertical shortening and extension. The NE-SW extension at this period is recorded in part by the formation adularia-filled veins (*46*), and recent Ar/Ar dates of the adularia indicate extension occurred 1.5 to 1.0 Ma (*45*). Chen *et al.* (*45*) propose that this stage of upper-crustal extension may have enhanced rock exhumation and accelerated the buildup the mountain topography. This

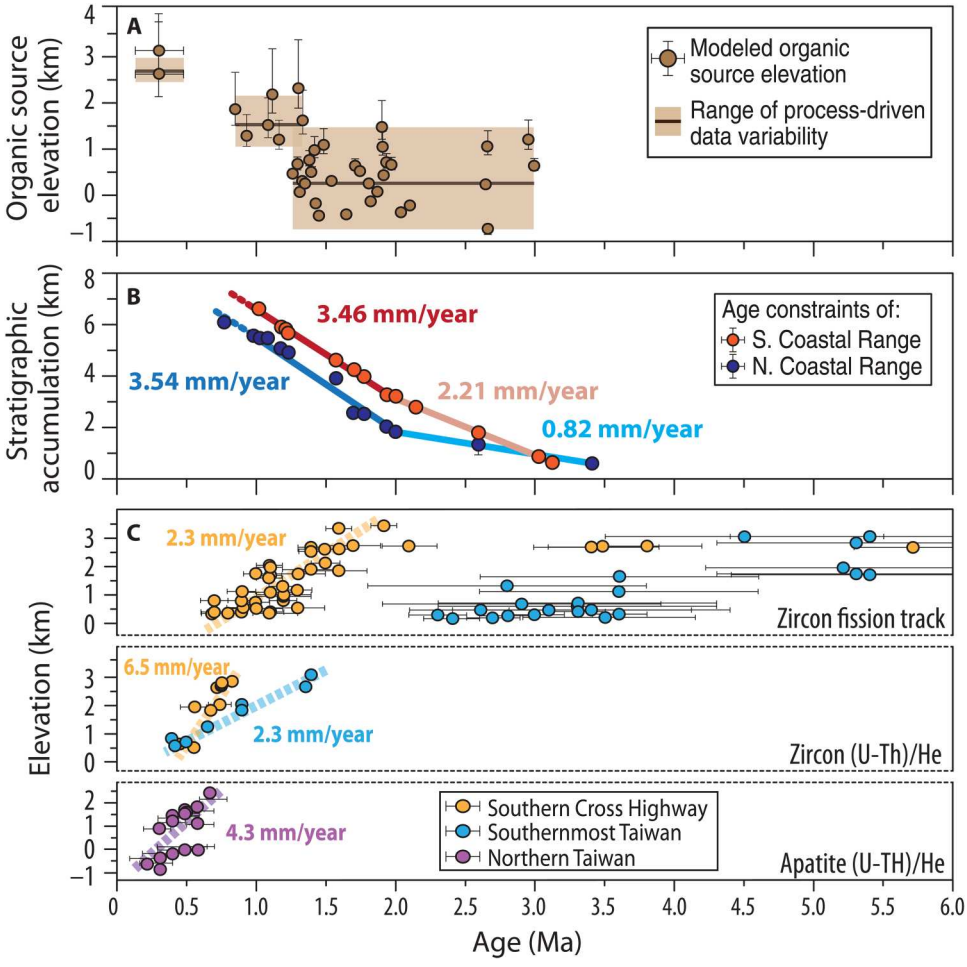

Fig. 5. Changes in organic source elevation, sedimentation rate, and thermochronological exhumation rate of the Taiwan orogenic belt. (**A**) Organic source elevation calculated from modeled $\Delta\delta^2$H-elevation relationship. (**B**) Sediment accumulation curves and calculated sediment accumulation rate from the marine turbidites in northern and southern Coastal Range modified after Lai *et al*. (*20*). (**C**) Age-elevation thermochronogy data and calculated exhumation rates from different transects in the Central Range modified after Hsu *et al*. (*13*) and Lee *et al*. (*18*). See fig. S4 for the locations of different transects.

interpretation could provide an explanation to the increase in mountain belt topography revealed by δ^2H_{nC29} data at ~1.3–1.5 Ma.

The rapid surface uplift of the Taiwan orogen at ~1.3–1.5 Ma or more recently at ~0.3 Ma may have contributed to the preservation of small areas of low relief found at both high and low elevations throughout the Central Range (*41*–*43*). Our data suggest that rapid topographic growth raised these surfaces to modern elevations in the Late Pleistocene and that the Taiwan landscape is still undergoing geomorphic adjustment to accelerations in both rock and surface uplift. These results highlight the power of the methods developed here to record rapid changes in paleotopography in tropical orogenic mountain ranges over geologic time scales and provide the first quantitative estimates of Taiwan paleotopography.

MATERIALS AND METHODS

Sedimentology and stratigraphy

On the basis of microfossil biostratigraphy and magnetostratigraphy data, the age of the Fanshuliao and Paliwan formations ranges from ~3 to ~0.78 Ma (*19*, *20*). Note that for the age model here, we used the same regression curve in (*20*), with the base of our stratigraphy column starting at the base of MKC section. The stratigraphy height has been corrected by adding 700 m. An angular unconformity was formed since ~0.5 Ma between the Paliwan Formation and the Pinanshan Conglomerate recording the rapid structural inversion and uplift to from modern Coastal Range (*48*). All river sections in this study represent a continuous, laterally extended sedimentary sequence in the same syn-collisional retro-foredeep basin of east Taiwan (*19*). The main three studied sections (MDJ, SSS, and BC) are widely considered as stratotypes for the Fanshuliao and Paliwan formations in the southern Coastal Range (*49*–*51*). These deposits are well correlated by widespread event marker beds (e.g., pebbly mudstone and tuff layers), and the result is consistent with magneto-biostratigraphic constraints (*52*, *53*). Paleoslope and paleocurrent data reveals that mud-rich sediment in this sedimentary basin that we focus on here are consistently derived from the northwest orogenic frontal slope throughout the whole basin-filling history (*19*). All existing sedimentological and stratigraphic evidence supports representativeness of our studied sections of

southern Coastal Range. For the Pinanshan Conglomerate, we adopt a depositional age of 0.303 ± 0.174 Ma. This age represents the mean of estimated deposition age for this unit, as constrained by the oldest age of lateritic soil (0.129 ± 0.012 Ma) developed on the oldest river terrace atop (*54*), and the maximum deposition age of the tilted conglomerate (0.476 ± 0.003 Ma) suggested by calcareous nannoplankton biostratigraphy (*55*, *56*).

Leaf wax *n*-alkane extraction

Siltstones and mudstones samples were collected using a stainless steel trowel and/or rock hammer and from freshly exposed rock outcrops that are free of any substantial modern or ancient organic material contamination by surface vegetation. Samples were freeze-dried for 24 hours and powdered with mortar and pestle before Soxhlet extraction. Approximately 150 g of sediment was extracted for 48 hours using a 400-ml mixture of dichloromethane:methanol (2:1, v/v). The total lipid extracts were saponified with 5 ml of 1 N potassium hydroxide (KOH) for 2 hours at 85°C to detach the fatty acids from ester lipids. After saponification, the neutral lipid fraction (N1) was further separated through silica gel column chromatography. Columns were filled with around 1.5 ml of activated silica gel and dried at 45°C and rinsed with hexane thoroughly before loading the column with the N1 split. Two milliliters of hexane (S1 fraction), 4 ml of dichloromethane (S2 fraction), and 4 ml of methanol (S3 fraction) were added sequentially to elute the N1 to obtain the nonpolar, midpolar, and polar fractions, respectively. After evaporative concentration, the nonpolar hexane fraction (S1) containing *n*-alkanes was further purified by urea adduction and silver nitrate ($AgNO_3$) chromatography to separate branched and cyclic alkanes. For urea adduction, 200 μl of urea-methanol solution, 200 μl of pentane, and 200 μl of acetone were added to the S1. The S1-containing fraction was frozen for at least 30 min to facilitate the crystallization of urea and compound adduction. The nonadducted fraction, which contains branched and cyclic alkanes, was rinsed and removed with hexane, and the adducted fraction (A1), which contains *n*-alkanes, was then obtained by adding H_2O: methanol (1:1, v/v) to dissolve the urea crystal and extracted with hexane. For the silver nitrate chromatography, the A1 was applied using columns filled with around 1.5 ml of $AgNO_3$ and eluted with 2 ml of hexane.

Molecular distributions and compound-specific δ^2H measurement

n-alkane abundances were quantified on a Thermo Fisher Scientific Trace Gas Chromatography (GC) Ultra with a flame ionization detector, using a BP5 column (inner diameter of 30 m by 0.25 mm and film thickness of 0.25 μm) with helium as the carrier gas at a constant flow rate of 1.5 ml/min. Individual alkanes were identified by comparing their retention time to an internal laboratory standard mixture of nC_7 to nC_{40}. The peak areas, denoted as *A*, of individual *n*-alkanes were used to calculate the molecular indices, carbon preference index (CPI), and average chain length (ACL), using the following equations (*57*)

$$\mathrm{CPI} = \frac{1}{2}\left[\frac{(A_{C25}+A_{C27}+A_{C29}+A_{C31})}{(A_{C24}+A_{C26}+A_{C28}+A_{C30})}+\frac{(A_{C25}+A_{C27}+A_{C29}+A_{C31})}{(A_{C26}+A_{C28}+A_{C30}+A_{C32})}\right] \quad (1)$$

$$\mathrm{ACL} = \left[\frac{(A_{C25}\times 25+A_{C27}\times 27+A_{C29}\times 29+A_{C31}\times 31+A_{C33}\times 33)}{(A_{C25}+A_{C27}+A_{C29}+A_{C31}+A_{C33})}\right] \quad (2)$$

The δ^2H of nC_{29} and nC_{31} were determined using a GC IsoLink II with a BP5 column (inner diameter of 30 m by 0.25 mm and film thickness of 0.25 μm), coupled to a Thermo Fisher Scientific MAT 253 isotope ratio mass spectrometer in the Stable Isotope and Organic Molecular Biogeochemistry Laboratory at the University of Connecticut. Compounds were separated on the GC with the temperature program set at 50°C for 1 min, ramped to 180°C at 12°C/min, and then ramped to 320°C at 5°C/min and held for 10 min. Isotopic compositions were standardized using a suite of *n*-alkanes from nC_{16} to nC_{30} in a standard mixture (Mix A7 from A. Schimmelmann Research Lab at Indiana University). We determined internal and external precision by repeatedly analyzing the standard of a range of sample sizes. The H3 factor was determined regularly through the period of analysis and was stable at ~7.9. During the interval of measurement, the Mix A7 standard was analyzed every four to five samples to account for size and scale effects. Repeat analyses throughout the run and for a range of standard concentrations yield a precision of <5‰ for δ^2H. All values are expressed in standard delta notation relative to Vienna standard mean ocean water.

We focus on nC_{29} for all discussions of changing topography here, as this is the most abundant compound throughout all samples. $\Delta\delta^2H_{nC31}$ is systematically depleted by ~10‰ relative to nC_{29} but shows the same general trend and overall magnitude of isotope depletion from Pliocene to recent (table S1).

Molecular alteration and isotopes

The distribution of *n*-alkane species reflects both environmental factors that affect plant biosynthesis processes as well as postdepositional processes related to molecular cracking. The distribution of molecular species can be expressed as indices such as CPI and ACL. Terrestrial plants typically produce *n*-alkanes with peak abundances from nC_{23} to nC_{33}, and in Taiwan, these are dominated by alkanes with 29 and 31 carbon atoms (*23*). In addition, plant-derived *n*-alkanes commonly show a strong odd over even preference in alkane distribution, which reflects the synthesis pathways (*57*–*60*).

There are a number of factors that influence sedimentary leaf waxes isotopic signals. First, different plant species are shown to have a highly variable offset between δ^2H_{nC29} and ambient water (*24*). A shift in apparent fractionation related to Pliocene-recent vegetation change could bias the δ^2H_{nC29} signal. However, Taiwan has maintained a tropical climate since the Pliocene (*33*) and C_3-dominant vegetation with little evidence for major ecosystem shift that could markedly change apparent fractionation patterns. Second, the reworking of detrital organic matter could introduce older organics from low-elevation sites, biasing the sedimentary δ^2H_{nC29} signal. However, southern Coastal Range sediments are derived from the high-pressure metamorphic core of the Central

Range, and analysis of Taiwan slates (this study) shows low to none nC_{29} that could bias our record. Third, microbial degradation and alteration during burial could shift the biomarker hydrogen isotope composition of older sediments toward enriched values (*57*, *60*). Alteration typically shifts ACL and CPI. Southern Coastal Range sediments have undergone a short burial duration and minimal heating in very low paleo-geotherm condition (14°C/km) in the sedimentary basin (*61*), and both ACL and CPI (table S1) show no evidence of alteration degradation with minimal change through the sequence and similar values to Late Pleistocene to modern marine sediments (*34*). These factors support the preservation of primary isotopic signatures of fluvially transported leaf waxes from the evolving orogen.

Source water isotope compositions correction

Seawater is the ultimate source of terrestrial precipitation. The variation in seawater δ^2H could therefore affect the isotopic composition of terrestrial precipitation. Seawater δ^2H has changed through the Pleistocene as a result of variations in global ice volume during glacial periods. Growth of terrestrial ice sheet results in heavy isotopic enrichment of the ocean reservoir, which, in turn, will cause increasing precipitation isotope ratio.

To constrain the variation in seawater isotope composition, we use planktonic foraminifera $\delta^{18}O$ records of the South China Sea (ODP 1148) (*35*) to constrain the variation in South China Seawater $\delta^{18}O$. This region in addition to the western Pacific, represent the primary moisture source areas for Taiwan. To convert planktonic foraminifera $\delta^{18}O$ to seawater $\delta^{18}O$, we calculate calcite-water fractionation [$\alpha_{calcite\text{-}H2O(l)}$] using the temperature-dependent fractionation factor equation

$$1000\ln\alpha_{calcite-H2O(l)} = 2.780 \times \frac{10^6}{T^2} - 2.890 \quad (3)$$

where, T is seawater temperature, which is constrained by the $U^{k'}_{37}$ sea surface temperature records of the South China Sea (ODP 1148) (*33*). The fractionation factor is then used with following equation to calculate local seawater $\delta^{18}O$ (*62*)

$$\delta^{18}O_{calcite} - \delta^{18}O_{H2O(l)} \cong 1000\ln\alpha_{calcite-H2O(l)} \quad (4)$$

For each data point, we calculate the changes in seawater $\delta^{18}O$ from modern seawater isotope composition. The changes in seawater and terrestrial precipitation δ^2H due to global ice volume variation then can be estimated according to the global meteoric water relationship, $\delta^2H = 8 \times \delta^{18}O + 10$ (*63*). The difference between seawater δ^2H of the past 3 Ma and present day is at a maximum of ~3‰, which is relatively small comparing to the magnitude of changes in δ^2H_{nC29} due to organic source elevation changes.

Supplementary Materials

This PDF file includes:

Figs. S1 to S4
Table S1

REFERENCES AND NOTES

1. P. England, P. Molnar, Surface uplift, uplift of rocks, and exhumation of rocks. *Geology* **18**, 1173–1177 (1990).
2. M. K. Clark, The significance of paleotopography. *Rev. Mineral. Geochem.* **66**, 1–21 (2007).
3. P. Molnar, P. England, Late Cenozoic uplift of mountain ranges and global climate change: Chicken or egg? *Nature* **346**, 29–34 (1990).
4. S. J. Dadson, N. Hovius, H. Chen, W. B. Dade, M.-L. Hsieh, S. D. Willett, J.-C. Hu, M.-J. Horng, M.-C. Chen, C. P. Stark, D. Lague, J.-C. Lin, Links between erosion, runoff variability and seismicity in the Taiwan orogen. *Nature* **426**, 648–651 (2003).
5. R. G. Hilton, A. Galy, N. Hovius, M.-C. Chen, M.-J. Horng, H. Chen, Tropical-cyclone-driven erosion of the terrestrial biosphere from mountains. *Nat. Geosci.* **1**, 759–762 (2008).
6. R. Emberson, A. Galy, N. Hovius, Weathering of reactive mineral phases in landslides acts as a source of carbon dioxide in mountain belts. *J. Geophys. Res. Earth Surf.* **123**, 2695–2713 (2018).
7. T. M. Blattmann, S.-L. Wang, M. Lupker, L. Märki, N. Haghipour, L. Wacker, L.-H. Chung, S. M. Bernasconi, M. Plötze, T. I. Eglinton, Sulphuric acid-mediated weathering on Taiwan buffers geological atmospheric carbon sinks. *Sci. Rep.* **9**, 2945 (2019).
8. Y. Park, P. Maffre, Y. Goddéris, F. A. Macdonald, E. S. C. Anttila, N. L. Swanson-Hysell, Emergence of the Southeast Asian islands as a driver for Neogene cooling. *Proc. Natl. Acad. Sci. U.S.A.* **117**, 25319–25326 (2020).
9. J. K. Caves Rugenstein, D. E. Ibarra, S. Zhang, N. J. Planavsky, F. von Blanckenburg, Isotope mass-balance constraints preclude that mafic weathering drove Neogene cooling. *Proc. Natl. Acad. Sci.* **118**, e2026345118 (2021).
10. T. Byrne, Y.-C. Chan, R.-J. Rau, C.-Y. Lu, Y.-H. Lee, Y.-J. Wang, The Arc–Continent Collision in Taiwan, in *Arc-Continent Collision*, D. Brown, P. D. Ryan, Eds. (Springer Berlin Heidelberg, Berlin, Heidelberg, 2011), pp. 213–245.
11. W. R. Chi, J. Namson, J. Suppe, Stratigraphic record of plate interactions in the Coastal Range of eastern Taiwan. *Mem. Geol. Soc. China* **4**, 155–194 (1981).
12. D. B. Stolar, S. D. Willett, D. R. Montgomery, Characterization of topographic steady state in Taiwan. *Earth Planet. Sci. Lett.* **261**, 421–431 (2007).
13. W. H. Hsu, T. B. Byrne, W. Ouimet, Y. H. Lee, Y. G. Chen, M. van Soest, K. Hodges, Pleistocene onset of rapid, punctuated exhumation in the eastern Central Range of the Taiwan orogenic belt. *Geology* **44**, 719–722 (2016).
14. L. Mesalles, F. Mouthereau, M. Bernet, C. P. Chang, A. T.-S. Lin, C. Fillon, X. Sengelen, From submarine continental accretion to arc-continent orogenic evolution: The thermal record in southern Taiwan. *Geology* **42**, 907–910 (2014).
15. T.-T. Shen, T.-K. Liu, S.-Y. Huang, P.-S. Hsieh, C.-Y. Wu, Post-collisional exhumation and geotherm pattern in northern Tananao Complex, northeastern Taiwan. *Terr. Atmospheric Ocean. Sci.* **31**, 369–381 (2020).
16. T. K. Liu, S. Hsieh, Y. G. Chen, W. S. Chen, Thermo-kinematic evolution of the Taiwan oblique-collision mountain belt as revealed by zircon fission track dating. *Earth Planet. Sci. Lett.* **186**, 45–56 (2001).
17. L. A. Kirstein, M. G. Fellin, S. D. Willett, A. Carter, Y.-G. Chen, J. I. Garver, D. C. Lee, Pliocene onset of rapid exhumation in Taiwan during arc-continent collision: New insights from detrital thermochronometry. *Basin Res.* **22**, 270–285 (2010).
18. Y.-H. Lee, T. B. Byrne, W. Lo, S.-J. Wang, S.-J. Tsao, C.-H. Chen, H.-C. Yu, X. Tan, M. van Soest, K. Hodges, L. Mesalles, H. Robinson, J. C. Fosdick, Out of sequence faulting in the backbone range, Taiwan: Implications for thickening and exhumation processes. *Earth Planet. Sci. Lett.* **594**, 117711 (2022).
19. L. S.-H. Lai, R. J. Dorsey, C.-S. Horng, W.-R. Chi, K.-S. Shea, J.-Y. Yen, Polygenetic mélange in the retrowedge foredeep of an active arc-continent collision, Coastal Range of eastern Taiwan. *Sediment. Geol.* **418**, 105901 (2021).
20. L. S.-H. Lai, R. J. Dorsey, C.-S. Horng, W.-R. Chi, K.-S. Shea, J.-Y. Yen, Extremely rapid up-and-down motions of island arc crust during arc-continent collision. *Commun. Earth Environ.* **3**, 100 (2022).
21. Y. Hsieh, C. Liu, J. Suppe, T. B. Byrne, S. Lallemand, The Chimei submarine canyon and fan: A record of Taiwan arc-continent collision on the rapidly deforming overriding plate. *Tectonics* **39**, e2020TC006148 (2020).
22. S. D. Willett, M. T. Brandon, On steady states in mountain belts. *Geology* **30**, 175 (2002).
23. M. Hren, W. Ouimet, Organic molecular paleohypsometry: A new approach to quantifying paleotopography and paleorelief. *Front. Earth Sci. China* **9**, 665324 (2021).
24. D. Sachse, I. Billault, G. J. Bowen, Y. Chikaraishi, T. E. Dawson, S. J. Feakins, K. H. Freeman, C. R. Magill, F. A. McInerney, M. T. J. van der Meer, P. Polissar, R. J. Robins, J. P. Sachs, H.-L. Schmidt, A. L. Sessions, J. W. C. White, J. B. West, A. Kahmen, Molecular paleohydrology: Interpreting the hydrogen-isotopic composition of lipid biomarkers from photosynthesizing organisms. *Annu. Rev. Earth Planet. Sci.* **40**, 221–249 (2012).
25. P. J. Polissar, K. H. Freeman, D. B. Rowley, F. A. McInerney, B. S. Currie, Paleoaltimetry of the Tibetan Plateau from D/H ratios of lipid biomarkers. *Earth Planet. Sci. Lett.* **287**, 64–76 (2009).
26. W. Dansgaard, Stable isotopes in precipitation. *Tellus A Dyn. Meteorol. Oceanogr.* **16**, 436–468 (1964).
27. C. Ponton, A. J. West, S. J. Feakins, V. Galy, Leaf wax biomarkers in transit record river catchment composition. *Geophys. Res. Lett.* **41**, 6420–6427 (2014).

28. V. Galy, T. Eglinton, C. France-Lanord, S. Sylva, The provenance of vegetation and environmental signatures encoded in vascular plant biomarkers carried by the Ganges–Brahmaputra rivers. *Earth Planet. Sci. Lett.* **304**, 1–12 (2011).
29. G. Zhuang, M. Pagani, C. Chamberlin, D. Strong, M. Vandergoes, Altitudinal shift in stable hydrogen isotopes and microbial tetraether distribution in soils from the Southern Alps, NZ: Implications for paleoclimatology and paleoaltimetry. *Org. Geochem.* **79**, 56–64 (2015).
30. T. I. Eglinton, V. V. Galy, J. D. Hemingway, X. Feng, H. Bao, T. M. Blattmann, A. F. Dickens, H. Gies, L. Giosan, N. Haghipour, P. Hou, M. Lupker, C. P. McIntyre, D. B. Montluçon, B. Peucker-Ehrenbrink, C. Ponton, E. Schefuß, M. S. Schwab, B. M. Voss, L. Wacker, Y. Wu, M. Zhao, Climate control on terrestrial biospheric carbon turnover. *Proc. Natl. Acad. Sci. U.S.A.* **118**, e2011585118 (2021).
31. D. B. Rowley, R. T. Pierrehumbert, B. S. Currie, A new approach to stable isotope-based paleoaltimetry: implications for paleoaltimetry and paleohypsometry of the High Himalaya since the Late Miocene. *Earth Planet. Sci. Lett.* **188**, 253–268 (2001).
32. D. B. Rowley, C. N. Garzione, Stable isotope-based paleoaltimetry. *Annu. Rev. Earth Planet. Sci.* **35**, 463–508 (2007).
33. G. Jia, F. Chen, P. Peng, Sea surface temperature differences between the western equatorial Pacific and northern South China Sea since the Pliocene and their paleoclimatic implications. *Geophys. Res. Lett.* **35**, L18609 (2008).
34. Q. Chang, M. Hren, A. T. Lin, C. Tabor, S.-W. Yu, Y. Eley, G. Harris, Terrestrial biomarker isotope records of late Quaternary climate and source-to-sink sediment transport processes in southwestern Taiwan. *Am. J. Sci.* **321**, 393–423 (2021).
35. Z. Jian, Q. Zhao, X. Cheng, J. Wang, P. Wang, X. Su, Pliocene–Pleistocene stable isotope and paleoceanographic changes in the northern South China Sea. *Palaeogeogr. Palaeoclimatol. Palaeoecol.* **193**, 425–442 (2003).
36. R. G. Hilton, A. Galy, N. Hovius, Riverine particulate organic carbon from an active mountain belt: Importance of landslides. *Global Biogeochem. Cycles* **22**, GB1017 (2008).
37. Y. Wang, H. Lu, K. Wang, Y. Wang, Y. Li, S. Clemens, H. Lv, Z. Huang, H. Wang, X. Hu, F. Lu, H. Zhang, Combined high- and low-latitude forcing of East Asian monsoon precipitation variability in the Pliocene warm period. *Sci. Adv.* **6**, eabc2414 (2020).
38. C. Y. Chen, S. D. Willett, M. Christl, J. B. H. Shyu, Drainage basin dynamics during the transition from early to mature orogeny in Southern Taiwan. *Earth Planet. Sci. Lett.* **562**, 116874 (2021).
39. J. Wang, J. D. Howarth, E. L. McClymont, A. L. Densmore, S. J. Fitzsimons, T. Croissant, D. R. Gröcke, M. D. West, E. L. Harvey, N. V. Frith, M. H. Garnett, R. G. Hilton, Long-term patterns of hillslope erosion by earthquake-induced landslides shape mountain landscapes. *Sci. Adv.* **6**, eaaz6446 (2020).
40. B. Campforts, C. M. Shobe, I. Overeem, G. E. Tucker, The art of landslides: How stochastic mass wasting shapes topography and influences landscape dynamics. *Case Rep. Med.* **127**, (2022).
41. D. Vohra, "Investigating Low-relief Topography in Taiwan's Central Range," thesis, University of Connecticut, CT (2022).
42. W. B. Ouimet, T. B. Byrne, L. L. Siame, P. R. Bierman, D. Rood, Slow Erosion Rates, Increasing Relief and Transient Landscape Evolution within the Central Range of Taiwan, paper presented at 2013 AGU Fall Meeting, San Francisco, CA, 9 to 13 December 2013.
43. M. L. Hsieh, A. Hogg, S. C. Kang, C. Y. Chou, The preservation of last-glacial (>50 to 40 ka) colluvium on low-relief surfaces in Alishan, an actively uplifting mountain in southwestern Taiwan. *Geomorphology* **322**, 159–174 (2018).
44. G.-R. Ho, T. B. Byrne, J.-C. Lee, L. Mesalles, C.-W. Lin, W. Lo, C.-P. Chang, A new interpretation of the metamorphic core in the Taiwan orogen: A regional-scale, left-lateral shear zone that accommodated highly oblique plate convergence in the Plio-Pleistocene. *Tectonophysics* **833**, 229332 (2022).
45. C.-T. Chen, C.-H. Lo, P.-L. Wang, L.-H. Lin, Extensional mountain building along convergent plate boundary: Insights from the active Taiwan mountain belt. *Geology* **50**, 1245–1249 (2022).
46. M. Chojnacki, "Late-stage Deformation and Exhumation of a High-pressure Metamorphic Belt in an Active Arc-continent Collision, Taiwan," thesis, University of Connecticut, CT (2019).
47. J. Wu, J. Suppe, R. Lu, R. Kanda, Philippine Sea and East Asian plate tectonics since 52 Ma constrained by new subducted slab reconstruction methods. *J. Geophys. Res. Solid Earth* **121**, 4670–4741 (2016).
48. N. Lundberg, R. J. Dorsey, Rapid Quaternary emergence, uplift, and denudation of the Coastal Range, eastern Taiwan. *Geology* **18**, 638–641 (1990).
49. R. J. Dorsey, N. Lundberg, Lithofacies analysis and basin reconstruction of the Plio-Pleistocene collisional basin, Coastal Range of eastern Taiwan. *Acta Geologica Taiwanica Science Reports of the National Taiwan University*, 57–132 (1988).
50. W. S. Chen, Tectonostratigraphic framework and age of the volcanic-arc and collision basins in the Coastal Range, eastern Taiwan. *Western Pacific Earth Sciences* **9**, 67–98 (2009).
51. C.-Y. Huang, W.-H. Chen, M.-H. Wang, C.-T. Lin, S. Yang, X. Li, M. Yu, X. Zhao, K.-M. Yang, C.-S. Liu, Y.-H. Hsieh, R. Harris, Juxtaposed sequence stratigraphy, temporal-spatial variations of sedimentation and development of modern-forming forearc Lichi Mélange in North Luzon Trough forearc basin onshore and offshore eastern Taiwan: An overview. *Earth Sci. Rev.* **182**, 102–140 (2018).
52. L. S. H. Lai, L. S. Teng, Stratigraphy and structure of the Tai-Yuan basin, southern Coastal Range, eastern Taiwan. *Bull. Central Geol. Surv. Ministry. Econom. Affairs. Taiwan.* **29**, 45–76 (2016).
53. L. S. H. Lai, T. W. Ng, L. S. Y. Teng, Stratigraphic correlation of tuffaceous and psephitic strata in the Paliwan Formation, Southern Coastal Range of Eastern Taiwan. *Bulletin of Central Geological Survey MOEA.* **31**, 1–32 (2018).
54. Y. H. Chu, "The Development of Red Soil and its Geomorphological Implication of the Southern Huatung Longitudinal Valley," thesis, National Taiwan University, Taipei (2012).
55. W. R. Chi, H. M. Huang, J.-C. Wu, Ages of the Milun and Pinanshan conglomerates and their bearing on the Quaternary movement of eastern Taiwan. *Proc. Geol. Soc. China.* **26**, 67–75 (1983).
56. C.-K. Chuang, L. Lo, C. Zeeden, Y.-M. Chou, K.-Y. Wei, C.-C. Shen, H.-S. Mii, Y.-P. Chang, Y.-H. Tung, Integrated stratigraphy of ODP Site 1115 (Solomon Sea, southwestern equatorial Pacific) over the past 3.2 Ma. *Mar. Micropaleontol.* **144**, 25–37 (2018).
57. C. Wang, Y. Eley, A. Oakes, M. Hren, Hydrogen isotope and molecular alteration of n-alkanes during heating in open and closed systems. *Org. Geochem.* **112**, 47–58 (2017).
58. G. Eglinton, R. J. Hamilton, Leaf epicuticular waxes. *Science* **156**, 1322–1335 (1967).
59. A. Vogts, H. Moossen, F. Rommerskirchen, J. Rullkötter, Distribution patterns and stable carbon isotopic composition of alkanes and alkan-1-ols from plant waxes of African rain forest and savanna C3 species. *Org. Geochem.* **40**, 1037–1054 (2009).
60. A. Brittingham, M. T. Hren, G. Hartman, Microbial alteration of the hydrogen and carbon isotopic composition of *n*-alkanes in sediments. *Org. Geochem.* **107**, 1–8 (2017).
61. R. J. Dorsey, E. J. Buchovecky, N. Lundberg, Clay mineralogy of Pliocene-Pleistocene mudstones, eastern Taiwan: Combined effects of burial diagenesis and provenance unroofing. *Geology* **16**, 944–947 (1988).
62. R. E. Criss, in *Principles of Stable Isotope Distribution* (Oxford University Press, USA, 1999).
63. H. Craig, Standard for reporting concentrations of deuterium and oxygen-18 in natural waters. *Science* **133**, 1833–1834 (1961).
64. C.-W. Lin, W.-S. Chang, S.-H. Liu, T.-T. Tsai, S.-P. Lee, Y.-C. Tsang, C.-L. Shieh, C.-M. Tseng, Landslides triggered by the 7 August 2009 Typhoon Morakot in southern Taiwan. *Eng. Geol.* **123**, 3–12 (2011).

Acknowledgments: We thank L.-H. Chang and J.-H. Shyu for their help on the field sample collection. **Funding:** This work was supported by NSF CAREER 1752815 to M.T.H. **Author contributions:** Q.C. and M.T.H. conceptualized the study. Q.C., M.T.H., L.S.-H.L., and R.J.D. conducted the field survey and sampling. Q.C. and M.T.H. conducted the laboratory analyses. Q.C., M.T.H., and L.S.-H.L. contributed to the figure preparation. All authors contributed to the manuscript preparation. **Competing interests:** The authors declare that they have no competing interests. **Data and materials availability:** All data needed to evaluate the conclusions in the paper are present in the paper and/or the Supplementary Materials.

Submitted 29 August 2022
Accepted 19 May 2023
Published 23 June 2023
10.1126/sciadv.ade6415

ScienceAdvances

Rapid topographic growth of the Taiwan orogen since ~1.3–1.5 Ma

Queenie Chang, Michael T. Hren, Larry Syu-Heng Lai, Rebecca J. Dorsey, and Timothy B. Byrne

Sci. Adv., **9** (25), eade6415.
DOI: 10.1126/sciadv.ade6415